Structural change of carbon supported Pt nanocatalyst subjected to a step-like potential cycling in PEM FC

Agnieszka Witkowska [a,*], Giorgia Greco [b], Sonia Dsoke [c], Roberto Marassi [c], Andrea Di Cicco [b]

[a] Department of Solid State Physics, Gdansk University of Technology, 80-233 Gdansk, Poland
[b] CNISM, School of Science and Technology, Physics Division, University of Camerino, I-62032 Camerino (MC), Italy
[c] Chemistry Department, University of Camerino, I-62032 Camerino (MC), Italy

ABSTRACT

In this paper we present detailed X-ray absorption fine structure (XAFS), X-ray diffraction (XRD) and transmission electron microscopy (TEM) investigations of the changes in the local geometric and electronic structure of Pt nanoparticles used as a cathode catalyst in proton exchange membrane fuel cell (PEMFC), working under controlled potential cycling conditions. The body of the results obtained suggests that in the first stage of PEMFC operation, small particle dissolution was a dominant process. Subsequent 100 h of work led to the progressive agglomeration of nanoparticles followed by a pronounced growth of the mean nanoparticle size. At the same time, high-quality XAFS spectra analysis demonstrated that negligible changes in structural local ordering and a slight increase in Pt 5d-electron density occurred during the whole FC operation period under consideration.

1. Introduction

Today the study of alternative energy sources is one of the main research subjects. Polymer electrolyte membrane (PEM) fuel cells (FCs) have the potential to solve many problems associated with the production and consumption of energy. Moreover, they may replace in the long term most current combustion systems in various energy end-use sectors, from portable power applications, electric vehicles to power plants [1,2]. Currently efforts and advances in FC technology are particularly focused on two major challenges: elongate lifetime and diminish cost. These two parameters strongly determine the fuel cell usage and unfortunately are often anti-correlated [3].

In this work we focus on the structural changes induced by real fuel cell working conditions observed in a pure Pt nanocatalyst supported on Vulcan (E-TEK). We intend to clarify which process among platinum particle recrystallization [4], Pt particle migration and agglomeration, platinum dissolution [5], or growth in nanoparticle size by dissolution–precipitation (Ostwald ripening) [6,7], is mostly responsible of the structural instability and performance loss of the cathode catalyst, one of the factors which strongly limit PEMFC durability.

To realize these aims we used techniques such as: XAFS (X-ray Absorption Fine Structure), to obtain unique information about the average local electronic structure and atomic arrangement around the catalytic metal site [8–11]; XRD (X-ray Diffraction), to control crystallization/amorphization effects and mean nanoparticle size

stability; HRTEM (High Resolution Transmission Electron Microscopy), to measure the size distribution of catalyst particles and also to observe micro- and nanoscopic changes observed in nanostructural metal and support.

The paper is organized as follows: in Section 2 catalytic layer preparation procedure and protocol applied to realize accelerated degradation are described; Section 3 contains experimental setup description; Section 4.1 is focused on the morphological and nano-scale catalyst characterization performed by XRD and TEM techniques. XAFS data and their analysis are presented in Section 4.2. In the final section, Section 5, the main conclusions of this work are drawn.

2. Materials

The catalytic layers were prepared using E-TEK 20%Pt supported on Vulcan XC-72 powder following the procedure described e.g. in [12]. The metal loading computed from the weight was about 0.9 mg/cm^2. The electrode obtained in such a way was cut on four small pieces (with area of 5 cm^2) and each piece was then put on the cathode side in a membrane electrode assembly (MEA) composed else of Nafion N-112® as a proton conductive membrane (thickness 50 μm) and Pt commercial electrode (Pt loading 0.5 mg/cm^2) as an anode. Four MEAs, not hot-pressed, and placed in a standard single fuel cell, were subjected to an accelerated test based on a step-like potential cycling [3]. The PEMFC was held for 1 h at 0.6 V and 1 h at open-circuit voltage (OCV) for a total time of 0, 50, 100 and 150 h. Other working conditions applied have been as follows: pure hydrogen (flux 100 ml/min) and pure oxygen (flux 200 ml/min) as a fuel on the anode and cathode side, respectively, $T(\text{cell/H}_2/\text{O}_2) = 70/70/70$ °C, $p(\text{O}_2) = p(\text{H}_2) = 1$ bar. The effective

* Corresponding author.
E-mail address: agnieszka@mif.pg.gda.pl (A. Witkowska).

working time was counted after 2 h of MEA conditioning. After selected working time, the electrochemical performance of the cell was checked and then MEA was demounted.

Subsequent stages of catalyst operation under potential cycling conditions showed a progressive loss of cell performance. The most pronounced change was observed after first 50 h of work (current density at 0.6 V decreased by more than 200 mA/cm^2).

3. Experimental details

Various state-of-the art material science techniques were used to study the micro- and nanoscopic properties of this nanomaterial including X-ray absorption fine structure (XAFS), X-ray diffraction (XRD) and transmission electron microscopy (TEM).

XRD patterns were obtained by a Philips diffractometer (PW1830 X-ray generator) with Bragg–Brentano geometry using Cu Kα radiation ($\lambda = 1.5406$ Å) monochromatized by means of a graphite crystal, TEM images were taken using a JOEL JEM-2100F at Institut de Minéralogie et de Physique des Milieux Condensés, UMPC (Paris, France) and XAFS spectra at the Pt L$_3$ edge were recorded at the Synchrotron Light Laboratory ELETTRA (XAFS station, Trieste, Italy) using a double-crystal monochromator equipped with Si(111) crystal [13]. All XAFS measurements were performed ex situ at room temperature. To obtain proper photoabsorber surface density and thickness for X-ray transmission measurements, samples were composed of an assembly of 6 layers of the electrode under consideration. The jump discontinuity at the Pt L$_3$-edge obtained in this way was in the 0.3–0.5 range.

4. Results and discussion

4.1. Morphological and nano-scale characterization

Detailed sample characterization is needed to perform a careful and reliable XAFS data analysis, especially if the final aim is to detect and study the changes in the local structure in ill-ordered systems [8,14,15]. The mesoscopic and nanoscopic characterization can also provide a new data for appropriate description of processes leading to catalyst degradation [5,16]. Therefore, considered cathodes were initially fully characterized by means of high resolution TEM and XRD measurements.

Typical TEM images of catalytic materials scraped from the electrodes aged for 0, 50, 100 and 150 h using step-like potential cycling procedure are presented in Figs. 1 and 2. A loss of uniformity in the spatial particle distributions (effects already detected and presented e.g. in [17]) is the main, directly appreciable, morphological change. Increasing number of metallic aggregates/large particles in subsequent stages can also be noted. Using high resolution TEM images it is possible to distinguish large particle from small particles agglomerate (see e.g. Fig. 2).

Performing detailed quantitative TEM micrograph analysis (with the help of ImageJ software [18]) the size distributions (SDs) of nanoparticles (considering the profile of more than 500 randomly selected quasi-spherically shaped particles) and mean metallic particle coverage (i.e. percent of the carbon support area covered by all Pt islands, C_{tot}, and covered only by nanoparticles with diameter smaller than 4 nm, C_s) were obtained. In all degradation stages the
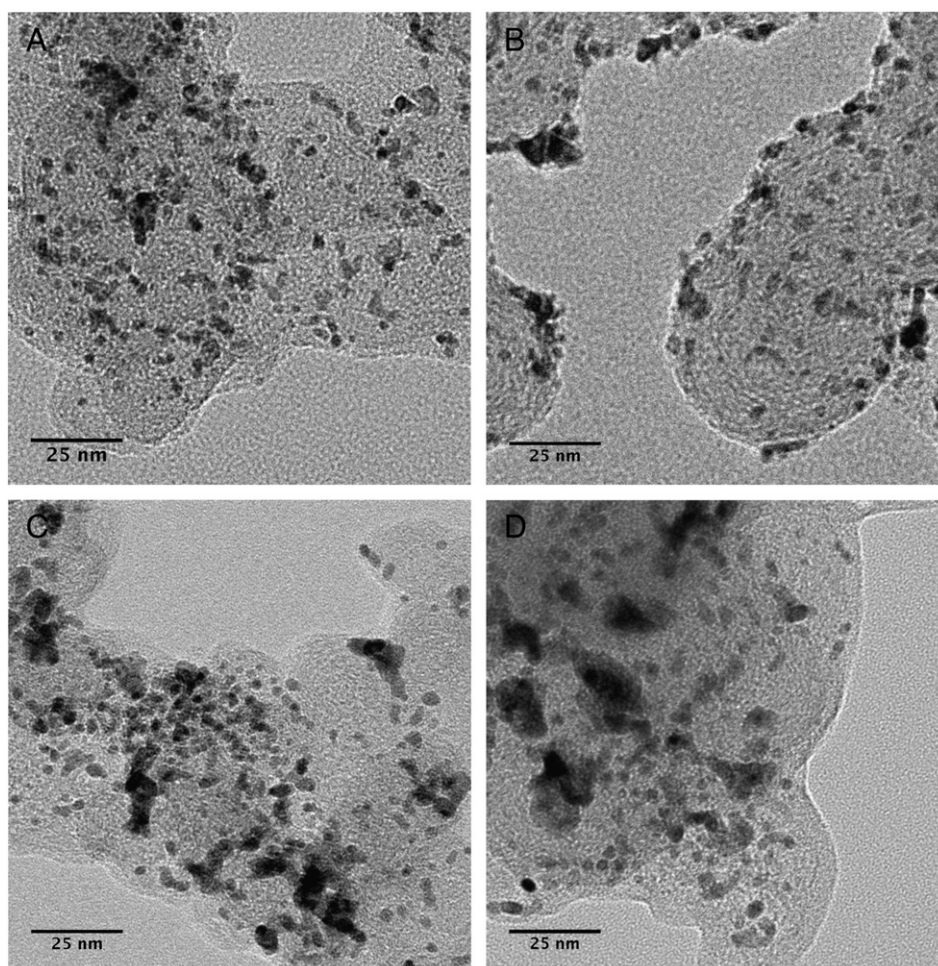

Fig. 1. TEM images of 20%Pt/Vulcan catalyst for electrodes used for A) 0 h, B) 50 h, C) 100 h and D) 150 h applying step-like potential cycling for monitoring the degradation process.
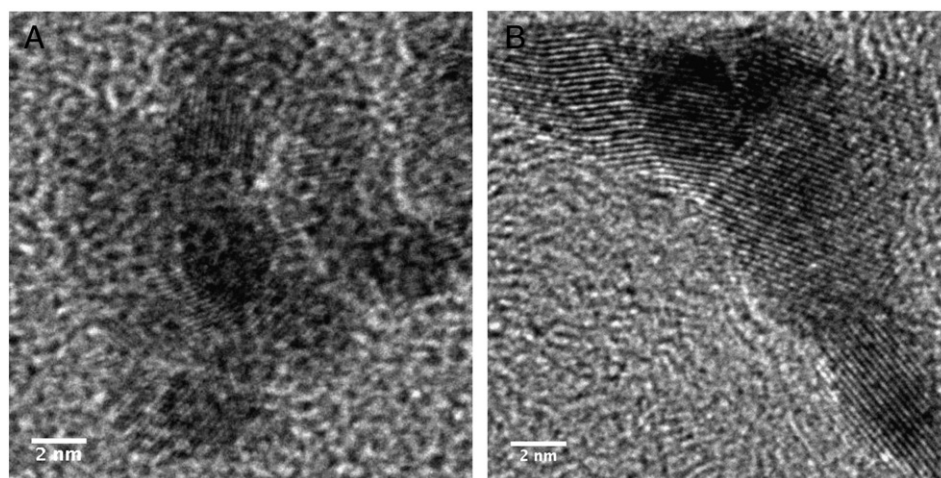
Fig. 2. HRTEM images of agglomerates observed in 20%Pt/Vulcan catalyst: PEM FC electrode used for A) 0 h and B) 100 h with step-like potential cycling. Lattice planes of Pt crystallites are clearly seen.
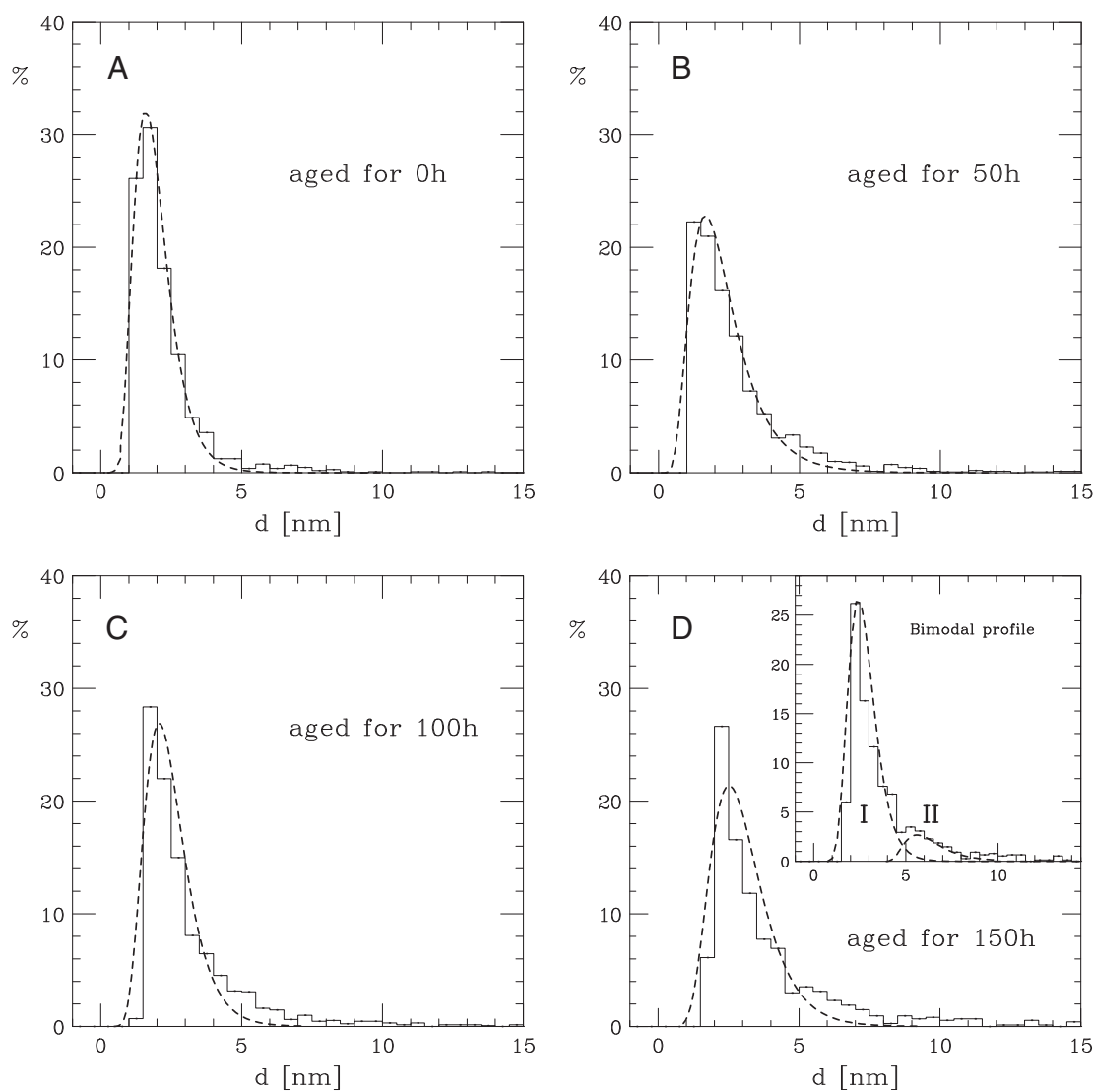

Fig. 3. Pt nanoparticle size distributions obtained by using TEM image-analysis of PEM FC electrode degraded for: A) 0 h, B) 50 h, C) 100 h and D) 150 h using step-like potential cycling. Dashed line—lognormal distribution used to describe SD. Inset in D)—SD decomposition by model of "bimodal" distribution profile.

obtained SD is asymmetric and shows a tail extended to large-sized nanoparticles. Therefore, SDs are reproduced through a lognormal model (see Fig. 3 and Table 1). However, it should be underlined that for catalysts aged for longer time than 50 h size distribution asymmetry is larger and one lognormal function is not enough to re-produce accurately the SD shape. Especially, the SD of catalysts aged for 150 h shows an almost "bimodal" profile (Fig. 3D).

We can infer from TEM data that the shift of the mean value in the SD, observed during the first working stage, is mainly associated with the dissolution of Pt particles having a diameter lower than 2 nm. Most of these particles were completely removed from the catalytic layer (note: both C_{tot} and C_s decreased of about 10% during the first 50 h of work). Moreover, the larger mean particle size and the broader SD distribution (see Table 1) suggest that during this degradation stage some of particles took part in an Ostwald ripening process [19]. On the other hand, following the model of Ascarelli et al. [20] this should also result in a decrease of the SD asymmetry. Instead, in our case we have observed an increase of the SD asymmetry. This deviation in SD shape can result by an extensive small particles diffusion into the ionomer phase where they were well separated from conducting carbon and could not take part in the classic Ostwald ripening process [16]. Thus, we can speculate that they could grow by migration and coalescence [21].

In the successive stage of catalyst work we observed a decrease in small particle coverage and virtually no change on the total amount of small particles (see Fig. 3, in catalyst aged for 100 h still about 85% of the particles are particles smaller than 4 nm). This can be easily ex-plained by still occurring processes of migration and agglomeration of Pt nanoparticles (within the ionomer phase and onto the carbon sup-port surface). After the last degradation stage, a further pronounced shift of the mean size value occurred. However, in this case it appears to be mainly caused by nanoparticle growth. It is difficult to determine which mechanism is mainly responsible for the change in SD shape and observed particle growth. Taking into account that the profile of SD has rather "bimodal" form (see inset in Fig. 3D) we can conclude that disso-lution–precipitation process was coupled with local coalescence of ag-glomerated particles [22].

In Fig. 4 we present the XRD patterns (free from a polynomial background) of the 20%Pt/Vulcan catalyst used for various working times, applying step-like potential cycling for monitoring the degra-dation process. The patterns were analyzed using a PEAKFIT program (whole-powder-pattern fitting program, see e.g. [23]). To estimate the Pt particle mean size and crystallite structure parameters peak line profiles were modeled with a Voigt function, using a Gaussian component to correct for instrument contribution to peak broadening ($\sigma_{corr} = 0.05°$). It was obtained that Pt particles display the reflection characteristics of fcc crystal structure with lattice parameter $a = 3.93(1)$ Å. The crystallite size determined by averaging the results of the (111), (200), (220) and (311) Bragg peak analysis changes as a function of catalyst working time (see d_{XRD} in Table 1). The diameters were estimated through Scherrer equation [24,25] with Scherrer
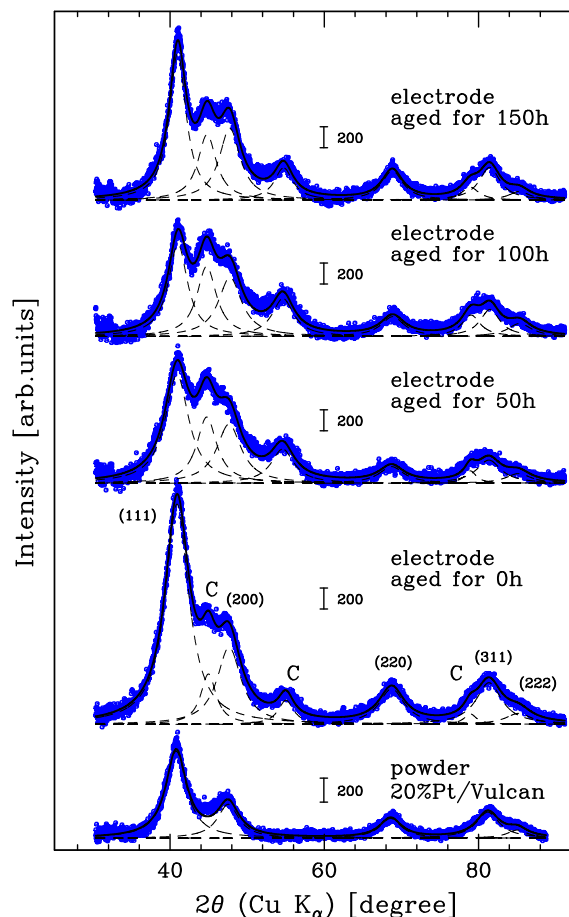

Fig. 4. X-ray diffraction patterns of 20%Pt/Vulcan catalyst. From bottom to top: powder form of catalyst (presented as a reference sample) and PEM FC electrodes aged for 0 h, 50 h, 100 h and 150 h using step-like potential cycling. Peaks signed as C correspond to the structure of the gas diffusion layer (carbon fiber cloth), part of the electrode which en-sures contact between MEA and FC graphite plate.

constant $K = 0.9$ (on the base of TEM data we accounted for relatively narrow SDs).

Mean particle sizes are found to be practically constant up to 50 h working time, while subsequent stages showed a gradual increase. This confirms that during the first stage of cell work small particle disso-lution involves only very small particles leading to their removal from the catalytic layer, as a main catalyst degradation process (see also [5]). Since XRD is a medium and long-range order sensitive method the contribution of the very small (or amorphous) particles (typically lower than ~ 2 nm) can be considered negligible. Taking into account the different natures of the probes, XRD and TEM results are consistent.

4.2. XAFS results

Fig. 5 shows the near edge XAFS region (XANES) of Pt L_3-edge spec-tra collected for PEM FC cathodes containing 20%Pt/Vulcan catalyst used 0 h, 50 h, 100 h and 150 h with step-like potential cycling. Close exam-ination of the figure (see also the inset) shows that the decrease in the white-line (WL) intensity is correlated with the increase of catalyst working time. The effect is mainly related to an increase in the 5d-electron occupancy of the absorber atoms. The most pronounced change is observed for the first working stage (WL peak area difference between $\mu_{electrode}$ and $\mu_{Pt-foil}$ is reduced by more than 20%) then WL in-tensity decreases gradually with time. However, these changes are greater than that expected from the increase in particle size (decrease in the surface-to-volume atom ratio).

Table 1
Results obtained for 20%Pt/Vulcan catalyst used in PEM FC for various working times with step-like potential cycling for monitoring the degradation process: d_{XRD} [nm]—mean par-ticle diameter as extracted from XRD pattern analysis; d_{TEM} [nm]—mean particle diameter, σ_{TEM} [nm]—standard deviation of the size distribution, C_{tot} [%]—mean total particle cover-age and C_s [%]—mean small particle (smaller than 4.0 nm) coverage as extracted from TEM image-analysis.

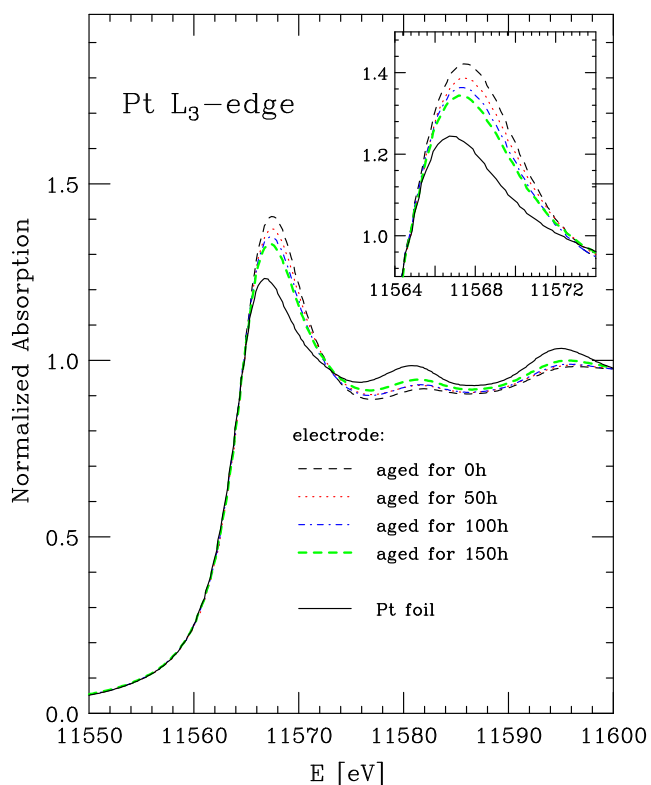| Working time	d_{XRD}	d_{TEM}	σ_{TEM}	C_{tot}	C_s
0 h	2.4 (1)	1.95 (3)	0.73 (3)	71	40
50 h	2.4 (1)	2.32 (8)	1.0 (1)	62	29
100 h	2.7 (2)	2.46 (9)	0.9 (1)	62	23
150 h	3.1 (2)	2.75 (3)[I]	0.8 (1)[I]	63	25
		6.36 (3)[II]	1.4 (1)[II]		

Fig. 5. Pt L$_3$ XANES spectra of 20%Pt/Vulcan catalyst aged in PEM FC for various times using step-like potential cycling. The spectrum of Pt foil was included for comparison.

in the framework of the GNXAS method [23,26,27] using advanced multiple-scattering simulations. The calculated EXAFS signal based on the fcc Pt crystalline structure was modeled using the first- and second-shell total two-body signals and two types of three-body contributions (configurations with vertex angle of 120° and collinear one). Details of the methodology applied to the EXAFS data analysis obtained for considered Pt nanostructured materials are described in [8].

Structural parameters for up to 4th shell were determined. The parameters of the first-neighbor two-body distributions were determined with higher accuracy, as they were used to compute most of the signals related to two-body and three-body configurations including first neighbors. For three-body and farther two-body distributions, the present parameter analysis gave only a qualitative description. Detailed best-fit results for the nearest two-body configurations obtained by using GNXAS method are presented in Table 2.

Looking at Fig. 6 we notice that EXAFS spectra are similar and only the signal amplitude (FT peaks intensity) increases as a working time increases. This is mainly due the increase of the mean coordination number (see Table 2), which is a natural consequence of the nanoparticle mean size growth. It is worth to note that the most pronounced changes in N_1 and N_2 values occur during the last considered stage of catalyst work. However, the most important observations are that only slight changes in the structural order parameters (slight order increase, better crystalline ordering) were obtained and no contribution of PtO configuration was detected (in any degradation stage). This means that in the case of carbon supported pure Pt nanocatalyst drop of FC performance is not due to changes in the local geometric structure. Degree of structural disorder does not affect, or at most affects in a negligible way, the electrochemical activity of the considered catalyst.

Additionally, referring to the results obtained for Pt$_{3\pm\delta}$Co/Vulcan nanocatalyst subjected to the same accelerated degradation test [9], we can conclude that the drop of catalyst activity in low temperature
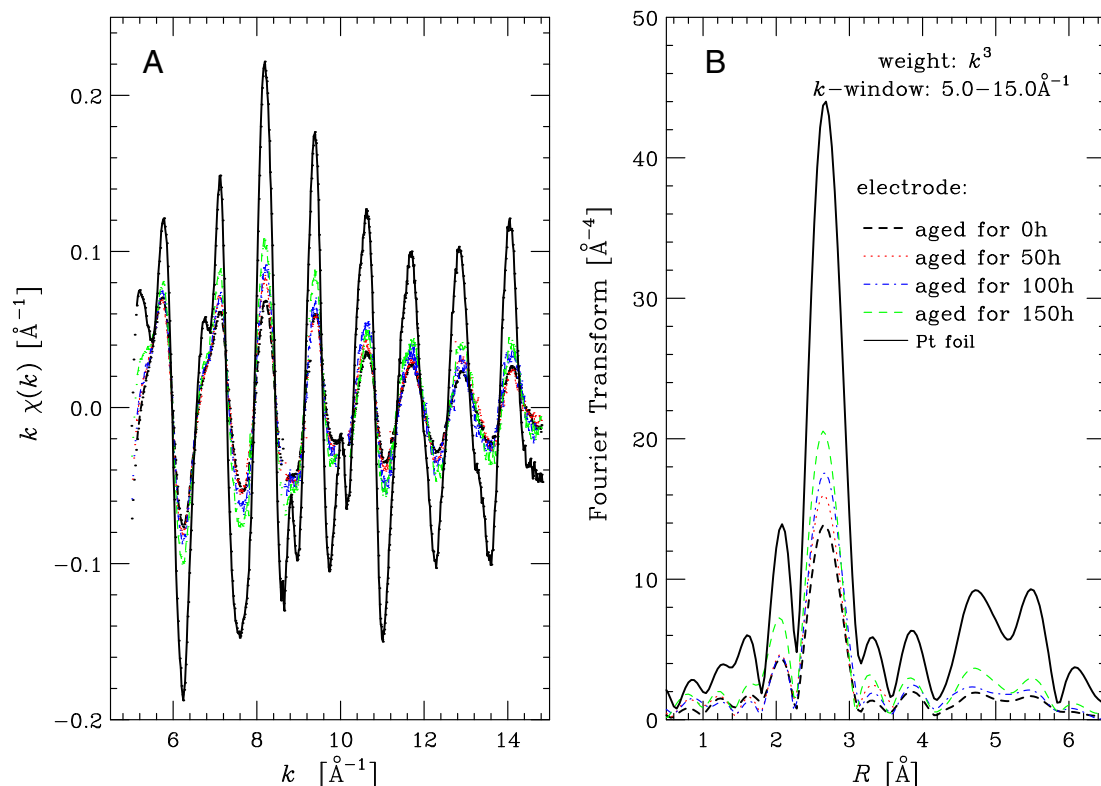
Fig. 6A and B shows the Pt L$_3$ extended XAFS spectra ($k\chi(k)$ EXAFS signals) and the corresponding Fourier Transforms (FTs) of the 20%Pt/Vulcan catalyst aged for various times. Data were analyzed

Fig. 6. A) Pt L$_3$ EXAFS spectra and B) corresponding Fourier Transforms of the 20%Pt/Vulcan catalyst aged in PEM FC for various time using step-like potential cycling. The spectrum of Pt foil was included for comparison.

Table 2
Structural parameters of Pt nearest two-body configurations as obtained using Pt L$_3$ spectra GNXAS analysis, for the 20%Pt/Vulcan catalyst aged in PEM FC by step-like potential cycling. Pt foil parameters are also shown for comparison [8]. R [Å]—the average inter-atomic distance, σ^2 [10^{-3} Å^2]—the standard deviation of distance, β—the skewness parameter, N—the coordination number.

Working time	R_1	σ_1^2	β_1	N_1	R_2	σ_2^2	β_2	N_2
0 h	2.761 (5)	8.5 (5)	0.3 (1)	9.6 (8)	3.92 (1)	12 (2)	0.2 (2)	4.5 (8)
50 h	2.762 (5)	8.1 (5)	0.3 (1)	9.8 (8)	3.93 (1)	11 (2)	0.1 (2)	4.6 (8)
100 h	2.763 (5)	7.4 (5)	0.2 (1)	10.1 (9)	3.91 (1)	11 (2)	0.1 (2)	4.7 (8)
150 h	2.763 (5)	7.3 (5)	0.3 (1)	10.6 (9)	3.92 (1)	11 (2)	0.1 (2)	5.2 (8)
Pt foil	2.766 (2)	4.9 (1)	0.0	12.0	3.909 (5)	7.4 (8)	0.0	6.0

fuel cells is predominantly caused by the active center dissolution [28] and nanoparticle growth. Local ordering plays a minor role in the activity enhancement/weakness.

5. Conclusions

In the present work, the results of the nanoscopic and atom level investigations of the structural changes induced by working conditions in carbon supported Pt nanoparticles used as a cathode catalyst in PEMFC are presented. The catalyst was subjected to an accelerated degradation test based on a step-like potential cycling leading to the gradual decrease of FC electrochemical performance, up to their almost complete deactivation after 150 h of operation. The electrochemical behavior has been correlated to the changes in nanoparticle size distribution, metallic phase coverage, Pt geometric and electronic structure detected by combined XAFS, TEM and XRD data analysis. Obtained results suggest that during the initial hours of work small Pt particle dissolution accompanied by the removing of these particles from the catalytically active region was a dominant catalyst degradation process. This process continued until particles having a size smaller than 2 nm disappeared. Then particle migration and agglomeration started to dominate leading to the increase of the nanoparticle size by dissolution–precipitation process coupled with a local coalescence of agglomerated particles. At the same time, no pronounced changes in Pt atom local structure was observed. Short-range structural order affects in a negligible way the electrochemical activity of the pure Pt nanocatalyst.

References

[1] V. Metha, J. Smith Cooper, J. Power Sources 114 (2002) 32–53.
[2] S. Litster, G. McLean, J. Power Sources 130 (2004) 61–76.
[3] R.L. Borup, J. Meyers, B. Pivovar, Y.S. Kim, R. Mukundan, N. Garland, D. Myers, M. Wilson, F. Garzon, D. Wood, P. Zelenay, K. More, K. Stroh, T. Zawodzinski, J. Boncella, J.E. McGrath, M. Inaba, K. Miyatake, M. Hori, K. Ota, Z. Ogumi, S. Miyata, A. Nishikata, Z. Siroma, Y. Uchimoto, K. Yasuda, K. Kimijima, N. Iwashita, Chem. Rev. 107 (2007) 3904–3951.
[4] P. Yu, M. Pemberton, P. Plasse, J. Power Sources 144 (2005) 11–20.
[5] K.J.J. Mayrhofer, J.C. Meier, S.J. Ashton, G.K.H. Wiberg, F. Kraus, M. Hanzlik, M. Arenz, Electrochem. Commun. 10 (2008) 1030–1033.
[6] H.R. Colón-Mercado, B.N. Popov, J. Power Sources 155 (2006) 253–263.
[7] R.L. Borup, J.R. Davey, F.H. Garzon, D.L. Wood, M.A. Inbody, J. Power Sources 163 (2006) 76–81.
[8] A. Witkowska, A. Di Cicco, E. Principi, Phys. Rev. B 76 (2007) 104110(12 pages).
[9] G. Greco, A. Witkowska, M. Minicucci, L. Olivi, E. Principi, S. Dsoke, A. Moretti, R. Marassi, A. Di Cicco, J. Phys. Chem. C 116 (2012) 12791–12802.
[10] L. Mino, G. Agostini, E. Borfecchia, D. Gianolio, A. Piovano, E. Gallo, C. Lamberti, J. Phys. D. Appl. Phys. 46 (2013) 423001.
[11] S. Bordiga, E. Groppo, G. Agostini, J.A. van Bokhoven, C. Lamberti, Chem. Rev. 113 (2013) 1736–1850.
[12] A. Witkowska, E. Principi, A. Di Cicco, S. Dsoke, R. Marassi, L. Olivi, M. Centazzo, V. Rossi Albertini, J. Non-Cryst. Solids 354 (2008) 4227–4232.
[13] A. Di Cicco, G. Aquilanti, M. Minicucci, E. Principi, N. Novello, A. Cognigni, L. Olivi, J. Phys. Conf. Ser. 190 (2009) 012043.
[14] A.I. Frenkel, Ch.W. Hills, R.G. Nuzzo, J. Phys. Chem. B 105 (2001) 12689.
[15] A.I. Frenkel, Z. Kristallogr. 222 (2007) 605.
[16] A.V. Virkar, Y. Zhou, J. Electrochem. Soc. 154 (6) (2007) B540–B547.
[17] E. Guilminot, A. Corcella, M. Chatenet, F. Maillard, F. Charlot, G. Berthomé, C. Iojoiu, J.-Y. Sanchez, E. Rossinot, E. Clauded, J. Electrochem. Soc. 154 (11) (2007) B1106–B1114.
[18] http://rsb.info.nih.gov/ij/.
[19] P.J. Ferreira, G.J. la O', Y. Shao-Horn, D. Morgan, R. Makharia, S. Kocha, H.A. Gasteiger, J. Electrochem. Soc. 152 (2005) A2256–2271.
[20] P. Ascarelli, V. Contini, R. Giorgi, J. Appl. Phys. 91 (2002) 4556–4561.
[21] M.A. Asoro, D. Kovar, Y. Shao-Horn, L.F. Allard, P.J. Ferreira, Nanotechnology 21 (2010) 025701.
[22] J. Xie, D.L. Wood, K.L. More, P. Atanassov, R.L. Borup, J. Electrochem. Soc. 152 (2005) A1011–A1020.
[23] A. Filipponi, A. Di Cicco, A. Trapananti, E. Principi, M. Minicucci, A. Witkowska, GNXAS Extended Suite of Programs for Advanced X-Ray Absorption Data-Analysis: Methodology and Practice, in: A. Di Cicco (Ed.), TASK Publishing, Gdansk, Poland, ISBN: 978-83-908112-8-4, 2009.
[24] P. Scherrer, Nachr. Ges. Wiss. Göttingen 26 (1918) 98–100.
[25] J.I. Langford, A.J.C. Wilson, J. Appl. Crystallogr. 11 (1978) 102–113.
[26] A. Filipponi, A. Di Cicco, C.R. Natoli, Phys. Rev. B 52 (1995) 15122–15134.
[27] A. Filipponi, A. Di Cicco, Phys. Rev. B 52 (1995) 15135–15149.
[28] Y. Shao-Horn, W.C. Sheng, S. Chen, P.J. Ferreira, E.F. Holby, D. Morgan, Top. Catal. 46 (2007) 285–305.